LA-7080-MS
Informal Report

412
2-15-78

AS. 1842

UC-4 and UC-25

Issued: December 1977

MASTER

Skull Melting of Synthetic Minerals

S. D. Scott
D. E. Hull
C. C. Herrick

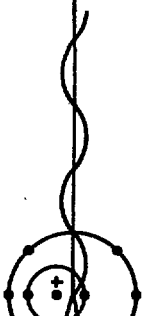

los alamos
scientific laboratory
of the University of California
LOS ALAMOS, NEW MEXICO 87545

An Affirmative Action/Equal Opportunity Employer

UNITED STATES
DEPARTMENT OF ENERGY
CONTRACT W-7405-ENG. 36

Printed in the United States of America. Available from
National Technical Information Service
U.S. Department of Commerce
5285 Port Royal Road
Springfield, VA 22161

Microfiche	$ 3.00	126-150	7.25	251-275	10.75	376-400	13.00	501-525	15.25
001-025	4.00	151-175	8.00	276-300	11.00	401-425	13.25	526-550	15.50
026-050	4.50	176-200	9.00	301-325	11.75	426-450	14.00	551-575	16.25
051-075	5.25	201-225	9.25	326-350	12.00	451-475	14.50	576-600	16.50
076-100	6.00	226-250	9.50	351-375	12.50	476-500	15.00	601-up	--1
101-125	6.50								

1. Add $2.50 for each additional 100-page increment from 601 pages up.

CONTENTS

SKULL MELTING OF SYNTHETIC MINERALS

by

S. D. Scott, D. E. Hull, and C. C. Herrick

ABSTRACT

Direct high-frequency induction melting of dielictric materials in a water-cooled cage has been developed in the synthetic minerals program at Los Alamos Scientific Laboratory. Molten material is contained in a skull, i.e., sintered shell, of its own composition so the traditional problems associated with refractory melt contamination are essentially eliminated. Preliminary analyses of power input, cage design, and coil geometry are discussed. Initial experimental results on the preparation of polycrystalline ingots, single crystals, and glasses are presented along with possible applications of this technique.

I. INTRODUCTION

In 1974, Russian scientists at the Lebedev Physical Institute[1] reported the development of a new process for melting kilogram quantities of refractory materials without either crucible or electrode contamination. Termed "skull melting" because of the sintered shell, or skull, of primary powder that encases the melt, the technique uses direct high-frequency induction heating of dielectric materials contained in a water-cooled cage.

Skull melting has been used in the fabrication of refractory single crystals, refractory glasses, and melt-cast ceramics with weights up to 25 kilograms. Further development of this technique can make a substantial contribution to:

1. studies of properties of melts at high temperature, chemical reactions in melts, solid-melt-gas equilibria, solidification of high-temperature melts and modeling of geothermal processes,
2. stable, corrosion-resistant, high-temperature materials for electrode lining for use in magneto-hydrodynamic generator channels, controlled thermonuclear fusion reactor walls and sheathing in continuously combusting automotive engines,
3. electrical heating elements which work at 2000°C,

4. refractory materials for use in pyrometallurgical processes,
5. preparation of solid electrolytes and semiconductors,
6. synthetic mineral single crystals for elastic constant measurements, fracture mechanics studies, and synthetic jewels,
7. encapsulating high-level radioactive waste products as stable, non-leachable ingots.

The application of skull melting to the production of a wide variety of new materials, with their corresponding large variation in electrical and thermal properties, will require a thorough understanding of the physics involved. Work completed at the Air Force Cambridge Research Laboratory by Wenkus and coworkers[2] established basic design criteria for skull melting apparatus, including simple geometrics for the water-cooled cage and power requirements for the RF (radio frequency) source. As part of the synthetic minerals program at LASL skull melting has been used in the preparation of forsterite, magnesia, hafnia, stabilized zirconia and thoria (Fig. 1). In support of these efforts a preliminary theoretical and experimental analysis of skull melting has been initiated. Attention has centered on:

1. the perturbation in applied magnetic fields produced by the water-cooled cage,
2. the functional dependence of power absorption by the melt and cage on conductivity and RF frequency,
3. the cage effect on coil inductance and its implications for new apparatus designs to produce large magnetic fields,
4. melt stability as a function of frequency,
5. operating procedures for initial melting and cooling procedures for single-crystal production.

This preliminary report summarizes results obtained during the spring and summer of 1977.

II. THE SKULL MELTING PROCESS

Typical skull melting configurations are illustrated in Figs. 2 and 3. Figure 2 depicts a concentrator-type cage melter--a cylindrical water-cooled unit with a thick sleeve near the center and a single slot to prevent eddy current closure. A water-cooled copper pedestal is positioned at the bottom to support a powdered charge. The dimensions shown do not correspond to any existing cage, but serve as a useful starting point for calculations of typical power losses and flux geometrics. Figure 3 shows a fingers-type cage melter, formed from nine water-cooled copper hairpins and a solid water-cooled bottom. The shown dimensions are those of the experimentally employed cage. Both cages are isolated from the three-to five-turn induction coil by a quartz sleeve.

Initially, the cage is filled with isostatically pressed oxide powder, topped by a small (approx. 1-to 2-in.-diam) graphite ring or a few grams of metal chips to serve as an initiator. Additions of loose powder are poured over the initiator (graphite ring or metal chips) to a depth of about 0.5 inch. The RF power (3-4 MHz) is slowly increased until a plate voltage of 5-6 kV is obtained. Within a few minutes, the initiator becomes incandescent and sufficient energy reaches the adjacent powder to cause melting. An increase in the RF-coil current indicates more efficient coupling occurred with the increase in electrical conductivity accompanying the phase transition from solid to molten oxide. The small seed melt absorbs sufficient power to melt adjacent powder, and within less than an hour, a large, stable melt can be obtained.

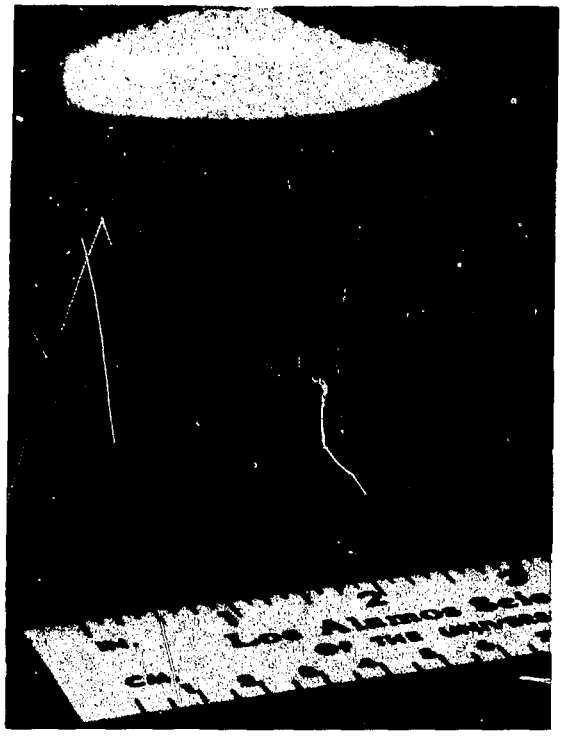

FORSTERITE

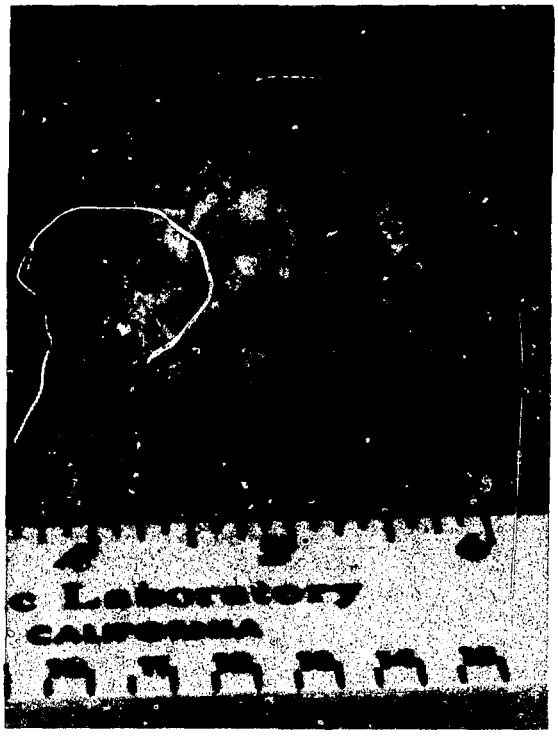

FUSED MgO

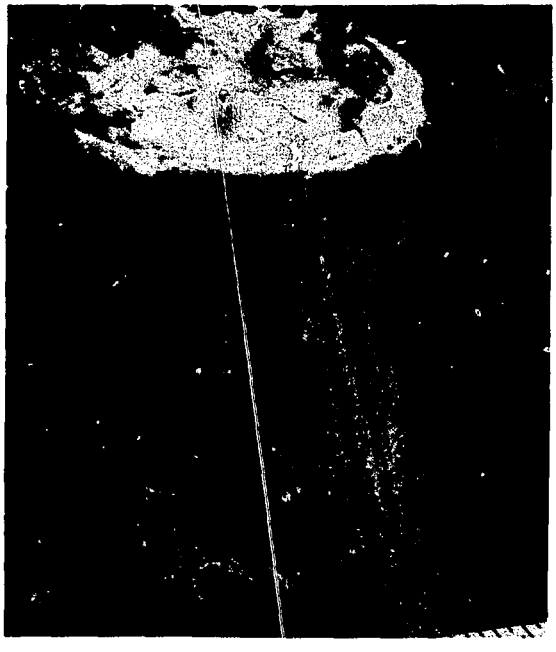

HAFNIA

ZIRCONIA

Fig. 1. Experimental results with skull melting.

THORIA SINGLE CRYSTALS

SINGLE CRYSTAL ThO_2

Fig. 1. (Cont)

At the upper oxide surface, molten oxide cannot be sustained because enormous radiation losses occur (3 kw/in^2 at 3000°C). Sintering takes place in this region yielding a hard shell that must be repeatedly punctured if feed powder is to be added.

The design and operation of a skull melting apparatus is restricted by several factors, that complicate the fusion of certain very refractory materials.

1. Arcing between cage fingers or to the RF coil. (The high voltages that exist between various components of the apparatus, coupled with the dusty environment, make the cage melter and coil susceptible to arcing, which reduces the power available to the melt and corrodes the wall material.)

2. Available power. (Very refractory materials such as thoria require a high-power input per unit volume to sustain the melt against thermal losses.)

3. Cage cooling capacity. (The cooling capacity of the cage is limited by the outlet water temperature. On occasion too much heat is conducted into the water lines, boiling ensues, cooling capacity drops, and the resulting pressure disrupts the O-ring seals, thus creating a hazardous situation.)

4. Outgassing. (Densification and melting are accompanied by continuous release of gas that is trapped beneath the hard skull. If the skull is not porous or periodically punctured, gas pressure will force molten oxide between the fingers, occasionally breaking the quartz, or the system will erupt, spewing molten material in all directions.)

5. Skin depth instability. (Early attempts to melt thoria (m.p.=3400°C) consistently failed after the seed melt had been established. The problem is thought to be associated with the skin depth (the distance over which the applied field attenuates a factor 1/e) of the molten charge, which at 3.6 MHz may be

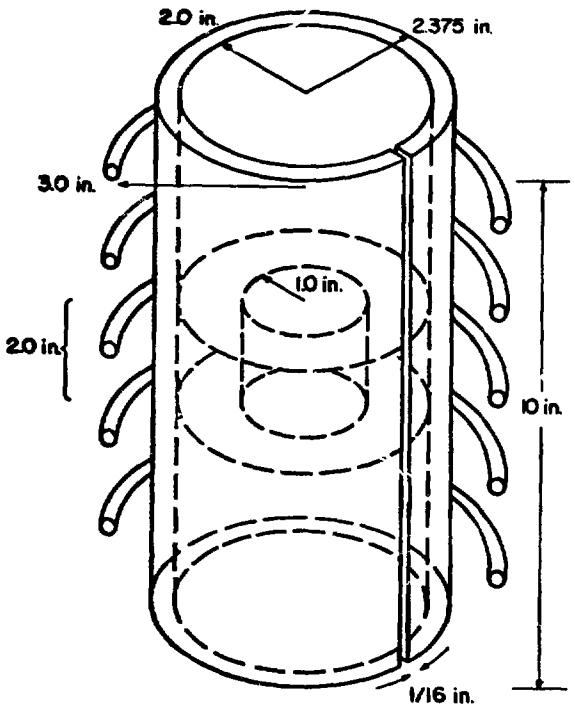

Fig. 2. Concentrator-type cage melter. All surfaces are water cooled. Five-turn coil carries 100 A.

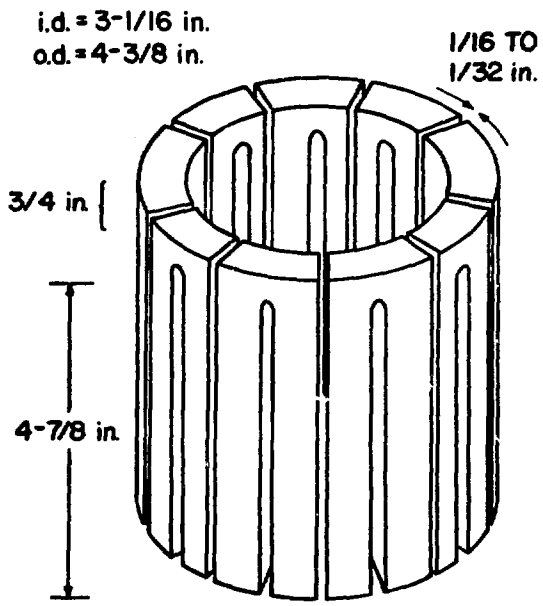

Fig. 3. Fingers-type cage melter. All copper surfaces, including solid bottom, are water cooled.

much smaller than the melt itself. This produces a melt geometry that is unstable when the skull is broken for feed powder additions.)

The experimenter has control over several groups of parameters which affect the melting performance, and which may be altered to alleviate operational problems. These are in coil geometry (number of turns, radius, and length), cage geometry, and RF-power generator capabilities. The coil geometry is easiest and cheapest to change. Cage modifications are more difficult and expensive to change, i.e., major design changes typically consume sixty hours of machining time. Some operating characteristics of the power supply, such as frequency, may be varied over a limited range through simple tuning circuits, but other characteristics such as an increase in maximum power require heavy investment. Therefore it is useful to understand the parametric behavior of a skull melting unit so its unique capabilities can be fully exploited at minimum cost and effort.

III. POWER INPUT TO CHARGE

An alternating magnetic field inside a material produces an electric field, which in turn induces electric currents in proportion to the electrical conductivity. These currents supply heat energy to the material through normal ohmic losses. The electrical conductivity of most solid refractory oxides is so low (10^{-12} -10^{-4} mho/m) that direct RF absorption is negligible, only a small fraction of a watt per cm^3 (cubic centimeter) for applied magnetic fields of several

thousand amperes/meter. Upon melting, the electrical conductivity increases dramatically (Fig. 4) and the oxides become effective RF power absorbers. The absorbed power sustains the melt against thermal losses by conduction and radiation, and melts additional powder adjacent to the melt. Thus it is sufficient to initially melt only a small portion of the charge for the process to continue by high-frequency energy absorption.

Raising an insulating powder from room temperature to its melting point can be accomplished by external heating sources such as electric arc, plasma jet, laser or radiation furnace, or internally by RF coupling to conducting metal chips or graphite. In principle, the external heating sources are preferable, because they cannot contaminate the melt. However, they are more expensive and, except in the case of a laser, difficult to install near a multikilowatt power source. Keem[3] (Purdue University) has initiated melts of thoria in a few minutes using a 300-watt CO_2 laser. At LASL oxide charges have been seeded with graphite rings or several grams of metal chips. The latter proved superior, yielding melts more reliably and with less contamination than graphite rings. The metal used is a component of the oxide. Initiation with metal chips is not always feasible, i.e., cerium oxides rapidly in air and is hazardous to machine, so without an external energy source one must at times be content with a graphite ring, followed by a long heating period to vaporize out the graphite impurity.

Survival of the initial melt depends on its initial geometry and volume, power input, thermal conductivity of the solid phase, heat transfer coefficient of the liquid-solid interface, and the solid and melt temperatures. Energy losses through conduction are approximately proportional to the surface area of the melt. Wenckus[2] showed that the molten region tends to assume the shape of a flattened body of revolution, with the major source of heat in a ring near the equatorial plane close to the surface of the body. The heat source is particularly concentrated on the melt surface if the skin depth of applied radiation, i.e., the distance over which the applied field attenuates a factor 1/e, is smaller than the melt dimensions. The skin depth

$$\delta = (2/\mu\omega\sigma)^{1/2}$$

of refractory oxides at 3 MHz varies from 10 centimeters to a fraction of a centimeter, depending on the conductivity σ, the frequency ω, and the permeability μ. Whatever the skin depth, the center of a melt absorbs relatively little RF power per unit volume, and is heated primarily by conduction from the outer regions.

For mathematical convenience Wenkus[2] approximated the shape of a molten region as an oblate spheroid of semimajor axes a and c:

$$\frac{r^2}{a^2} + \frac{Z^2}{c^2} = 1 ,$$

where r and Z are the horizontal and vertical coordinates. For $\delta >> c$, the uniform magnetic field H_o, produced by the coil, penetrates the melt with little distortion, and the absorbed power is

$$W_1 = \frac{\pi\sigma\mu_o^2\omega^2 a^4 c H_o^2}{15} = \frac{2\pi}{15}\frac{\mu_o\omega a^4 c H_o^2}{\delta^2} . \qquad (1)$$

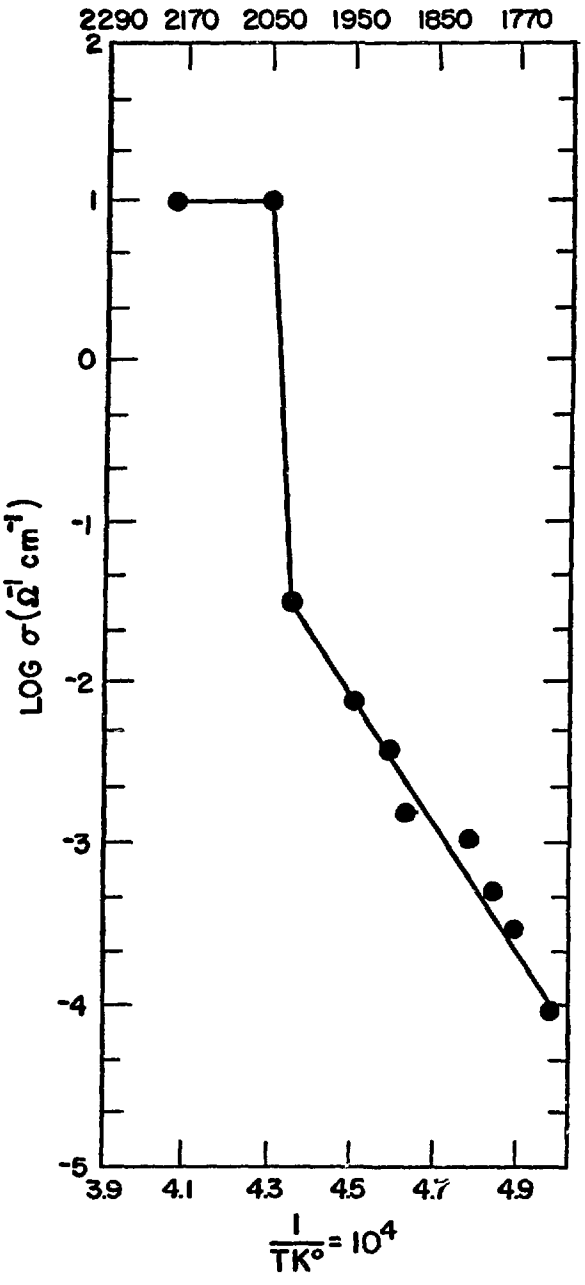

Fig. 4. Temperature dependence of electrical conductivity of Al_2O_3.

As a numerical example we take the following values:

σ = 1000 mho/meter
a = .0222 meter
c = a/4
H_o = 4175 ampere-turns/meter
$\omega = 2\pi\ (3 \times 10^6)$ Hz
δ = 0.0092 meter $\approx 2c$
$\mu_o = 4\pi \cdot 10^{-7}$

then W_1 = 2755 watts. The values of H_o and ω are those of the concentrator-type cage melter with "a" chosen for a 7/8-in. melt radius; the conductivity is a handbook value for molten zirconia. It is important to note that, for $\delta >> c$, the power loss

1. increases linearly with the conductivity σ,
2. depends strongly on the melt dimensions a^4c, and
3. is proportional to $\omega^2 H_o^2$.

The strong dependence on melt dimensions determines the smallest melt that can be sustained for a given magnetic field. Thus when initiating a melt, it is advantageous to position the metal chips in a ring of maximum radius (perpendicular to the magnetic field) so as to create a melt with a large major semiaxis. The $\omega^2 H_o^2$ factor in Eq. (1) would imply that the power input increases with the square of the frequency, but for a constant voltage drop across the RF coil, the axial magnetic field H varies approximately as $1/\omega$, hence over a wide range of frequencies the power input is independent of frequency. At very low frequencies H falls faster than $1/\omega$ and the power input is diminished.

At high frequencies where $\delta << c$, the magnetic field is excluded from the interior of the melt, and the power absorbed by the melt surface is

$$W_2 = \frac{H_o^2 a^2}{2\sigma\delta} F(c/a) = \frac{H_o^2 a^2}{2} \left(\frac{\omega\mu_o}{2\sigma}\right)^{1/2} F(c/a) , \qquad (2)$$

where F(c/a) is a geometry function which is essentially constant over the interval c/a = 0.1 to 1.0 (see Table I). Assuming the same material properties and dimensions as in the $\delta >> c$ example, the skin depth δ becomes equal to c at a frequency of 10.13 MHz. For a constant potential drop across the RF coil, H is reduced to 1236 ampere/meter at 10.13 MHz and the power input is W_2 = 506 watts.

If the coil voltage at 10.13 MHz were increased to produce the same magnetic field as at 3 MHz the power input necessary would be W_2 = 5769 watts.

Equations (1) and (2) show that as σ varies from small to large values, due to temperature variations, the power absorbed passes through a maximum which, for the parameters chosen, lies between 2800 and 5800 watts.

Several experiments with isostatically pressed thoria powder, using a three-turn coil at 3.4 MHz and 20 kw applied power, terminated abruptly when the melt cooled and solidified after addition of feed powder. Examination of the charge revealed a hollow, glass-lined oblate spheroid, with a thick base containing a few single crystals and thoria glass, encased in a thick skull of sintered thoria. This geometry is consistent with the assumption of a small skin depth for molten thoria, which would produce a thin molten shell with the interior powder heated only by conduction and radiation. The result would be a growth of crystals along the vertical walls and a settling of the interior powder on the bottom of the void. Furthermore, should the thin layer of melt be broken by a charge of cold feed material or by puncturing the skull, the system would become unstable, and the complete cooling observed becomes predictable.

This hypothesis was tested by melting thoria at 2.6 MHz. Although the calculated increase in skin depth, attributable to the frequency, is a mere 20%, a stable 3500-gram melt was obtained and held for over five hours.

This experiment suggests that for optimum performance and stable operation, the skin depth should be approximately equal to the melt radius. Under this condition, the power input to the melt for a constant voltage drop is nearly maximized. Because the experimenter has no control over the melt's intrinsic electrical and magnetic properties, the skin depth parameter can only be influenced through the RF frequency. Even among a restricted class of materials such as refractory oxides, there is an enormous variation (orders of magnitude) in conductivity; hence an RF generator, or a set of them, with broad frequency capability is necessary for experimental purposes.

IV. CAGE GEOMETRY

A multiturn coil operated at a frequency of several megahertz produces a strong magnetic field in the interior that is approximately constant throughout the volume, and directed along the axis of the coil. Since the alternating magnetic field is the power source for a melt, it is of interest to determine how the cage structure alters the applied field. The conclusion is that, except near the solid bottom of a cage, the magnetic field geometry is entirely unaffected by the presence of the cage, but the magnitude of the field may be substantially increased through a reduction in coil inductance. Arcing problems between components of the cage can be remedied in the fingers-type cage by using a large number of hairpin fingers. For the single-slotted concentrator-type cage the arcing problem is essentially insoluble and places a severe constraint on the magnitude of magnetic field that can be attained.

TABLE I

GEOMETRICAL FACTOR F(c/a)

c/a	F(c/a)
0.0001	24.020
0.001	18.101
0.01	12.534
0.1	8.190
0.2	7.510
0.25	7.465
0.4	7.564
0.6	8.121
0.8	8.744
1.0	9.425

A. Flux Geometry

When electromagnetic fields with frequencies in the megahertz range impinge upon conducting surfaces, they induce surface currents which cancel the incident field inside the material. Alternating electric and magnetic fields are thereby excluded from the conductor except in a thin layer (specified by the skin depth) near the surface. In MKS units the surface current $\underset{\sim}{K}$ is given by

$$\underset{\sim}{K} = \underset{\sim}{n} \times \underset{\sim}{H}$$

where $\underset{\sim}{H}$ is the magnetic field at the surface and $\underset{\sim}{n}$ is a unit normal to the surface. $\underset{\sim}{H}$ satisfies

$$\underset{\sim}{H} \cdot \underset{\sim}{n} = 0$$

at all conducting surfaces, i.e., it has no component normal to the surface. In both cage designs, the current induced in the outside walls is equal in magnitude to the applied $\underset{\sim}{H}$ field, and is directed in the θ direction. These currents loop around the inside of the cage structure, producing a magnetic field nearly identical to the field outside. It is tempting to draw an analogy between the magnetic flux lines in a concentrator-type cage and the velocity field in a constricted water line, but the analogy is false. The slot in the concentrator forces continuity between currents on the inner and outer surfaces, hence the fields inside and out are nearly identical. Viewed differently, the slot allows magnetic field lines to slip out of the cage as they approach the constricting sleeve.

B. Computer Program

The magnetic field $\underset{\sim}{H}$ satisfies the wave equation

$$(\nabla^2 + K^2)\ \underset{\sim}{H} = 0 \qquad (3)$$

where $K = \omega/c$ everywhere in space. Because the normal component of $\underset{\sim}{H}$ must vanish at all surfaces of the cage, ∇ is of the order $1/r_o$ where r_o is some characteristic dimension of the cage, typically 0.1 meter. At 3 MHz, $K = 2\pi/100$ meter, hence $\nabla^2 \simeq 100/m^2$ and $K^2 \simeq 0.004/m^2$. Evidently $\nabla^2 >> K^2$, so to a good approximation $\nabla^2 \underset{\sim}{H} = 0$ inside the cage.* This approximation is equivalent to neglecting

*Note this approximation is not valid for the case of a hollow cylinder with no slot. For such a geometry the magnetic field is attenuated inside, hence the gradients in the interior are much less than the estimate H/r_o as given.

the time rate of change of magnetic field in Maxwell's equation

$$\nabla \times \underset{\sim}{E} = - \dot{\underset{\sim}{B}} \ .$$

On conducting surfaces $\dot{B}$ is not negligible, and this is reflected in the boundary conditions $\underset{\sim}{n} \cdot \underset{\sim}{H} = 0$, $\underset{\sim}{n} \times \underset{\sim}{H} = \underset{\sim}{K}$.

To facilitate computer solution of the system,

$$\nabla^2 \underset{\sim}{H} = 0$$
$$\underset{\sim}{H} \cdot \underset{\sim}{n} = 0$$

at all conducting surfaces, we write $\underset{\sim}{H} = - \nabla\phi$. Then

$$\nabla^2 \phi = 0 \qquad (4)$$
$$\partial\phi/\partial n = 0 \quad \text{at all conducting surfaces.}$$

A computer code written by John Hayes[4] for the solution of $\nabla^2\phi = 0$ in axisymmetric systems with Neumann or Dirichlet boundary conditions was modified for use in solving the system (4). While the code satisfied all the Maxwell equations to a good approximation, it does not impose the constraint of continuity of current on the inner and outer surfaces. Furthermore, being an axisymmetric code it cannot allow flux lines to pass through a slot along the length of the cage. Thus, once the flux lines enter the top of the cage, the code forces them to remain inside the cage, resulting in an artificial magnification of magnetic field intensity within the constricting sleeve of the concentrator. Nonetheless, the program provides a fairly accurate description of the field geometry, and the numerical results are useful for comparison with analytical expressions.

Computer-generated plots of the magnetic flux lines for the sample concentrator cage and coil configuration are shown in Figs. 5 and 6. Note especially the dead space near the inner sleeve where the magnetic field intensity is

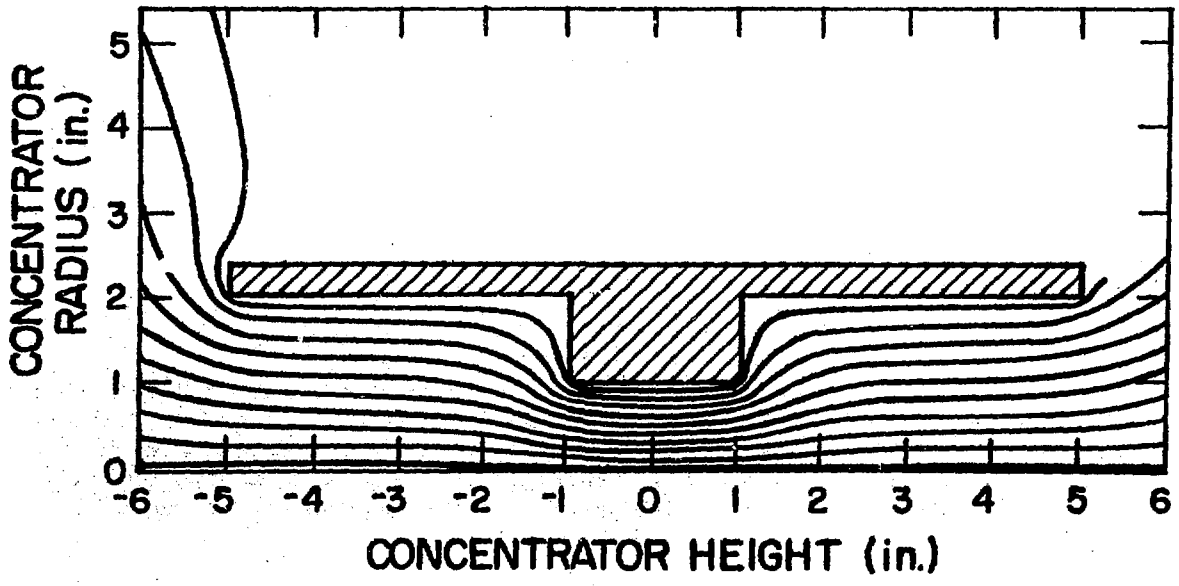

Fig. 5. Magnetic flux lines for sample concentrator coils at -2, -1, 0, 1, and 2 in.

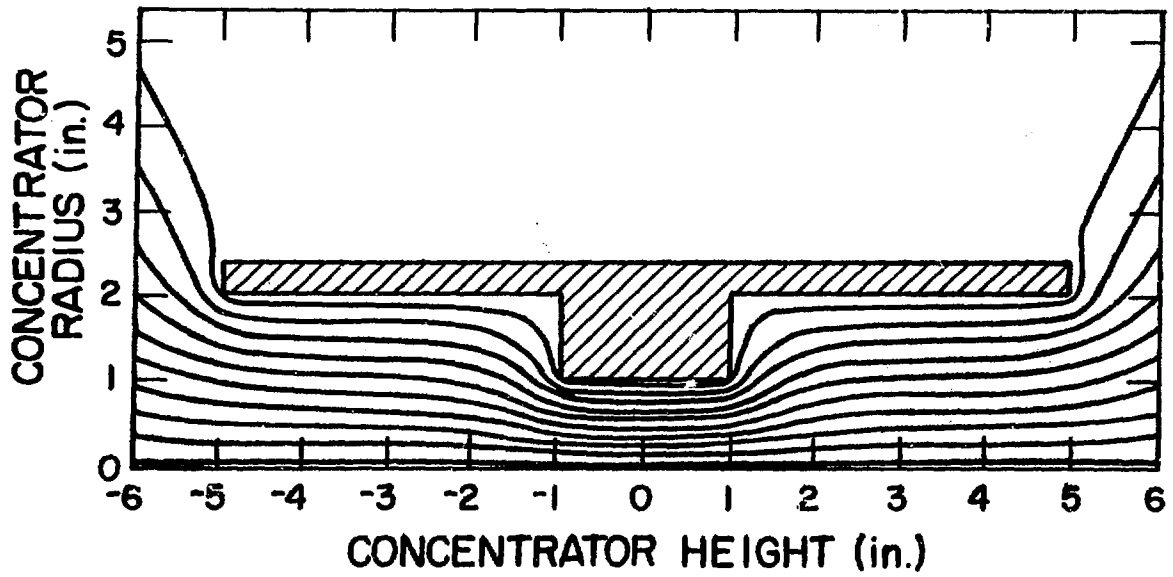

Fig. 6. Magnetic field lines for sample concentrator coils at 0, 1, 2, 3, and 4 in.

very small -- stable melts cannot be maintained in these regions because insufficient power is available. As expected, the assumed cage axisymmetry prevents any flux lines from leaking out the sides of the cage, and results in an artificially high calculated magnetic field intensity within the constricting sleeve (see the Appendix).

C. Fields Near Cage Bottom

At the solid bottom of a cage melter the Z-component of the magnetic field must vanish. Along all vertical walls B_z is approximately constant and equal to the B-field outside the cage. The current distribution in the hairpin fingers, viewed from the top, is shown in Fig. 7.

The effective current distribution may be approximated by a cylindrical current sheet. In the interior region the governing equation for B is,

$$\nabla^2 \underset{\sim}{B} = 0$$

and

$$\nabla^2 B_z = 0 \ .$$

Very far from the bottom of the finger, $B = \mu_o I$ where I is the current per unit length in the walls. Let $B_z = \mu_o I$ and, say, $z = 20\ r_o$ be a boundary condition. (The choice of boundary condition is not important when one is far from the region of interest.) The the system to be solved is

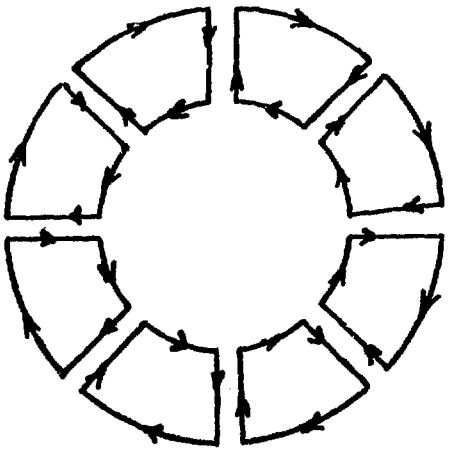

Fig. 7. Induced currents in cage fingers (top view).

$$\nabla^2 B_z = 0$$

with $B_z = \mu_o I$ at $r = r_o$

$B_z = \mu_o I$ at $Z = 20 r_o$

$B_z = 0$ at $Z = 0$

The solution is

$$B_z = \frac{4\mu_o I}{\pi}\left(\sum_{n=o}^{\infty} \frac{\sin((2n+1)\pi\ t/20\ I_o}{(2n+1)\ I_o} \cdot \frac{((2n+1)\ \pi\ S/20}{((2n+1)\ \pi/20)}\right)$$

$$+ 2\mu_o\ I \sum_{n=1}^{\infty} \frac{J_o(\chi_n S)\ \sinh\ (\chi_n t)}{J_1\ (\chi_n)\ \sinh\ (20\ \chi_n)\ \chi_n}$$

where

$S = r/r_o$

$t = Z/r_o$

I_o = First modified Bessel function

J_o = First Bessel function

J_1 = Second Bessel function

$X_n = n^{th}$ root of J_o

The RF power available to a melt varies as B_Z^2. In Fig. 8 equipotential lines of $B_Z^2/(B_Z^2)_{max}$ are plotted in the region S = 0 to 1 and t = 0 to 2. It can be seen that 80% of maximum available power is attained at distances greater than a single radius from the bottom.

D. Arcing Between Fingers on Slotted Surfaces

The changing magnetic field inside the cage induces electric fields, which are sometimes strong enough to cause arcing between components of the cage. Assuming a uniform, axial magnetic field $\underset{\sim}{H}$ inside the cage, the potential difference induced around a circular loop C in Fig. 9 is

$$|\Delta V| = \int_C \underset{\sim}{E} \cdot d\underset{\sim}{l} = \int \underset{\sim}{B} \cdot d\underset{\sim}{a} = \omega\mu H\ \pi r_o^2 .$$

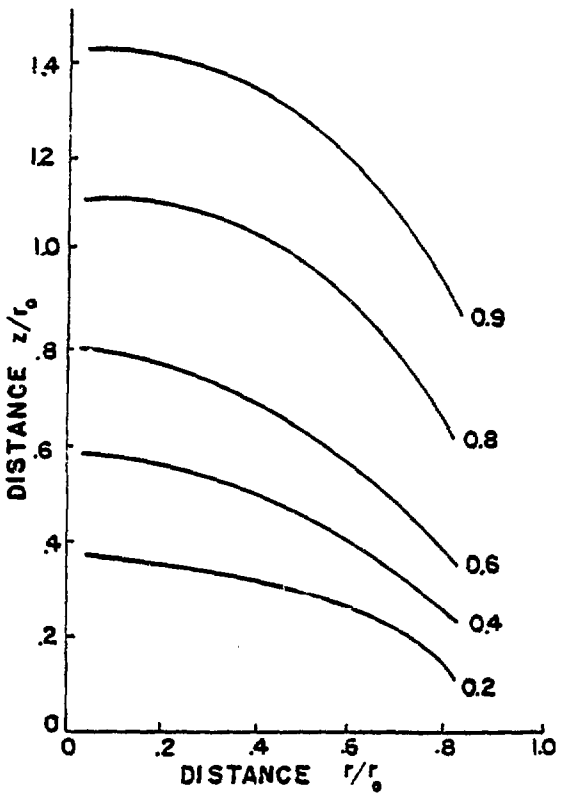

Fig. 8. Fraction of maximum available rf power near bottom of cage melter (equipotential lines of B_z^2).

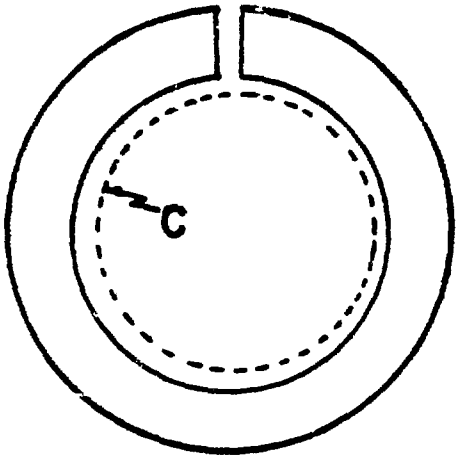

Fig. 9. Cage Concentrator (Top View).

The surface current K produces a potential drop around the cage wall that is a factor r_o/δ smaller than $|\Delta V|$, so the entire potential difference $|\Delta V|$ occurs between the two slotted surfaces. In a fingers arrangement, the potential difference is $\Delta V/N_f$, where N_f is the number of fingers, i.e.,

$$\Delta V = \omega\mu H\pi r_o^2/N_f \ .$$

For a 5-turn coil of 3-in. radius and 4-in. length, carrying an average current of 100 amperes, the potential difference across a 4-in.-diam cage is

$$\Delta V = 802 \text{ volts}/N_f .$$

With a typical single slot of width .0625 in., the electric field between the slot surfaces would be twelve kilovolts per inch, which, in a dusty environment as found in these experiments, is sufficient to initiate arcing between the slots. The distinct advantage of a finger-type cage arises from the reduction in slot voltage and consequently, the arcing problem is negated.

E. Power Loss and Resistive Loading of Cage

The power absorbed by a conducting surface per unit area is

$$\partial P/\partial A = |H|^2/2\sigma\delta \ .$$

The magnetic field H is approximately

$$H = K(R/S)\ N_c I/S \ ,$$

where N_c is the number of coil turns, R the coil radius, S the coil length, I the current, and K(R/S) a geometrical factor (see Table II). Total absorbed power is then given by

$$P = N_c^2 A_c K^2(R/S) I^2/2\sigma \delta S^2 ,$$

where A_c is the area of the cage, parallel to the Z - axis that lies within the volume of the coil. The series resistance introduced by the cage is

$$R = N^2 A_c K^2(R/S) /\sigma\delta S^2 .$$

For our sample concentrator-type cage and a 5-turn, 100-ampere coil,

$$P = 277 \text{ watts}$$
$$R = .0277 \text{ ohm}$$

Using elliptic integrals, we can obtain an exact expression for the magnetic field anywhere inside or outside the coil, in the absence of a cage. Numerically integrating the field over the cage area, one obtains for the power loss P = 271 watts and R = .0271 ohms.

F. Reduction in Coil Inductance

The cage walls effectively exclude all electric and magnetic fields from the interior region, i.e., the water-cooled channels. This has the effect of reducing the field energy of the coil, which may be written

$$E_{field} = 1/2\ LI^2,$$

where L is the self-inductance of the coil and I the current amplitude. If the cage occupies a volume, V_{cage}, inside the coil, the field energy and the self-inductance are reduced by a factor $(V_{coil} - V_{cage}) / V_{coil}$.

TABLE II

GEOMETRICAL FACTOR K(R/S)

R/S	K
0	1.0
.2	.85
.4	.74
.6	.65
.8	.58
1.0	.53
1.5	.43
2.0	.37
4.0	.24
10.1	.12

This reduction in coil inductance is very important because the coil inductance is primarily responsible for the impedance of the coil-cage system. For frequencies above 10^5 hertz, the coil current is well approximated by

$$I = \Delta V_{RF}/i\omega L ,$$

where ΔV_{RF} is the potential drop across the coil. Decreasing the coil inductance increases the coil current for a given potential drop across the coils. Because power density increases as the square of the coil current, substantially higher temperatures can be maintained in a cage that occupies a significant fraction of the coil volume.

V. POWER SUPPLY AND COIL GEOMETRY

A. Power Absorption

The RF coil, as well as the cage, absorbs power due to the presence of alternating electric and magnetic fields at the surface. Power loss per unit area is the same as that for the cage.

$$\partial P/\partial a = K^2/2\sigma\delta ,$$

where K, the surface current, is $I/2\pi r_c$ and r_c is the minor coil radius. Total power absorption is then

$$P_{coil} = \frac{N_c I^2 R}{2\sigma\delta r_c} ,$$

where R is the major coil radius. For the standard 5-turn, 100-ampere coil operated at 3 megahertz, this power is 171 watts.

B. Coil Geometry

As mentioned earlier, the inductance of an N-turn coil of length S and radius R is

$$L_{coil} = \frac{K(R/S)\mu_o N^2 \pi R^2}{S} \cdot \frac{V_{coil}-V_{cage}}{V_{coil}} .$$

The impedence of the system is dominated by the coil inductance, hence

$$I = \Delta V/i\omega L = \frac{S\Delta V}{\mu_o N^2 \pi R^2 \omega K(R/S)} \cdot \frac{V_{coil}}{(V_{coil}-V_{cage})} .$$

A typical magnetic field inside the coil is

$$H = K(R/S)N\ I/S, \text{ or}$$

$$|H_{fl}| = \frac{|\Delta V|}{\mu_o N \pi R^2 \omega} \cdot \frac{V_{coil}}{V_{coil}-V_{cage}} . \qquad (5)$$

Thus to increase H for a given power supply, one has the option of reducing the number of coil turns, N, decreasing the coil radius, decreasing the frequency, or building a new cage to occupy a greater volume fraction of the coil. Large magnetic fields are necessary to melt very refractory materials or those with small electrical conductivities. Substituting Eq. (5) into Eq. (1), the power input to the melt (for $\delta >> c$) can be written as

$$P_{melt} = \frac{2\sigma\, a^4 c |\Delta V|^2}{15\pi N^2 R^4} \quad . \tag{6}$$

If we make the crude assumption that the melt radius a is proportional to the coil radius R (the maximum melt radius is the cage radius, which must be less than the coil radius), and the height of the melt is proportional to the coil length, then

$$P_{melt} \simeq \frac{\sigma S |\Delta V|^2}{N^2} \quad .$$

Thermal losses from the melt are proportional to the melt surface area, hence

$$\frac{P_{melt}}{P_{loss}} = \frac{\sigma S |\Delta V|^2}{N^2 R(R+S)} \quad .$$

If a seed melt can be established but does not densify and melt the exterior regions, it may be necessary to increase the P_{melt}/P_{loss} ratio by increasing the coil voltage or decreasing the number of coil turns. If a seed melt cannot be established, then "a" and "c" are not proportional to R and S and Eq. (5) suggests that the power input may be increased by (1) increasing the coil voltage ΔV, (2) decreasing the number of turns N, or (3) decreasing the coil radius R.

VI. OPERATING HINTS

During the course of these experiments several techniques were devised to efficiently initiate melts and lower the operational hazards. Some are listed below.

(1) The importance of isostatically pressing the initial charge cannot be over emphasized. The block serves as a solid base on which the seed melt can form without a large volume change destabilizing the melt. If the solid charge is sized to fit the cage snugly it also acts as a barrier to prevent molten material from discharging between the fingers.

(2) If there is a gap between the initial charge and the cage wall, it should be filled with compacted powder. Molten material invariably destroys the quartz insulator and the ensuing arcing badly damages the equipment.

(3) A melt should be fabricated starting at the bottom by periodically adding powder. This is most easily and safely accomplished by pouring powder over the exposed skull to a 1/2-in. depth, waiting a few minutes for the powder to heat and degas, then pressing the feed through the skull with a ceramic or graphite-tipped insulating rod. One should endeavor to maintain a thin, porous skull to allow continuous outgassing during densification and feed powder melting.

(4) The quartz insulating sleeve should be flared at the top edge to prevent ejected melt or powder from settling on the RF coils.

VII. EXPERIMENTAL RESULTS

The purpose of these experiments was twofold: first to develop the experimental capability and second to apply the technique to real problems such as growing large single crystals of geological interest for dynamic measurements, determining the feasibility of encapsulating high-level radioactive wastes in synthetic minerals, preparing new materials for drill bits, and producing reproducible specimens for mechanical testing.

Experimental RF generators operating at 3.4 MHz and 0.5 MHz were borrowed for these experiments. Materials melted during the course of these preliminary experiments are listed in Table III.

Magnetite (Fe_3O_4) and Uraninite ($UO_{2\pm x}$) were melted in a horizontally mounted, single-slotted, water-cooled concentrator with a 2x3 in. opening. Presumably the semiconducting properties of these materials were responsible for their absorption of 400 kHz energy. Attempts to melt the other substances in this manner were unsuccessful.

Magnesia melted when the single-slot cage was positioned vertically and subjected to 26 kW at 3.2 MHz using a 4-turn coil. A sintered MgO block, which served as the container floor, melted after twenty minutes at temperature. The released molten oxide flowed into a water-cooled cylinder and froze, thereby suggesting the use of a removable plug for casting fused ceramics. The remaining materials were melted in the water-cooled finger-type cage shown in Fig. 3.

A chromia glass was melted. The "seed" melt survived but a stable melt was not produced. Because this powder could not be isostatically pressed, the poor results can be attributed to the volume change on melting and the gases released during melting.

Early attempts to fuse thoria yielded similar results but when the frequency was reduced to 2.6 MHz a stable melt was produced and contained for over five hours. Outgassing problems forced termination of the experiment. The product was a large fused thoria ingot weighing 1875 grams, which will require a diamond wheel in a radioactive area for cutting.

Hafnia and zirconia "seed" melts transformed easily into stable melts. Powdered hafnia was manually added to its melt until the entire cage volume (28 in.) was filled with the molten material. The ingot was cut with a diamond

TABLE III

MATERIALS MELTED

Material	Melting Point (°C)	Amount (g)
Fe_3O_4	1550	~3
$UO_{2\pm x}$	2878	~3
MgO	2880	~400
ThO_2	3400	~3500
$ZrO_2 \cdot CaO$	2690	~2400
$2MgO \cdot SiO_2$	1900	~774
$.65SiO_2 \cdot .175Cr_2O_3 \cdot .175BaO$	?	~500
HfO_2	2790	3142

wheel, revealing a large crystalline region near the bottom and a glassy yellowish region near the top. The zirconia run yielded a large quantity of sintered and glassy zirconia, encasing a single crystalline region totalling 583 grams. The crystalline region was free from holes and microcracks, and consisted of small (mm-size) single crystals. The bulk density of the crystalline block was 6.26 g/cm^3, which agrees with the literature value for cubic zirconia.

Forsterite (Mg_2SiO_4) was fused using loose powder and a graphite ring. The low melting temperature (1900°C) and porous skull combination made this particular melt a comparatively easy experiment to perform.

Figure 1 shows some of the results of this investigation. The single crystal of stabilized zirconia was obtained from Wenkus through John Keem. After the Air Force Cambridge Research Laboratory terminated their skull melting research the principle investigator acquired the RF equipment and is now marketing stabilized zirconia single crystals as synthetic diamonds.

VIII. CONCLUSIONS AND RECOMMENDATIONS

1. The utility of skull melting as a technique for melting kilogram quantities of refractory compounds without contamination by crucible walls has been fully demonstrated. The process is safe, fairly inexpensive, and simple enough to avoid high labor costs.

2. A parametric study of the physics of skull melting has been initiated. The important variables have been identified, and their effects on the system have been calculated.

3. The power radiated by the coil as a function of frequency and coil geometry remains poorly understood. The radiated power subtracts from the power available to the melt, and may require substantial shielding to prevent interference with radio communications.

4. An instability in melt geometry due to small skin depth has been identified. To produce stable melts of a wide variety of materials, it will be necessary to obtain an RF generator with a broad frequency capability (10MHz-0.5MHz).

5. The feasibility of melting and recrystallizing thoria in kilogram quantities has been verified. This represents the first step in developing a process to encapsulate high-level radioactive waste in non-leaching synthetic minerals.

6. Pure macroscopic crystalline blocks of synthetic minerals free from microcracks can be fabricated in a skull melting apparatus for use in fracture mechanics studies.

REFERENCES

1. V. I. Aleksandrav, V. V. Osiko, H. M. Prokhorov, and V. M. Tatarintsev, "A New Method for Obtaining Refractory Single Crystals and Fused Ceramics," translated from Vestnik Acad. Nauk SSR 12, 29 (1973).

2. J. F. Wenkus, M. L. Cohen, A. G. Emslie, W. P. Minaski, and P. F. Strong, "Study, Design and Fabricate a Cold Crucible System," Air Force Cambridge Research Laboratories report AFCRL-TR-75-0213 (February 1975).

3. John Keem, Purdue University, personal communication, May 1977.

4. J. K. Hayes "Four Computer Programs Using Green's Third Formula to Numerically Solve Laplace's Equation in Inhomogeneous Media," Los Alamos Scientific Laboratory report LA-4423 (June 1970).

APPENDIX

The listed results are the root mean square (RMS) values of the B_z and B_r fields in the absence of the cage (theory) and with a cage present. For these calculations a five-turn coil with turns at 0, 1, 2, 3, 4 inches was used. The coil position relative to that of the cage is measured from the cage center where Z = 0 in.

Z = 4.75 INCHES

Radius (cm)	B_z (Tesla)	B_z (Theory)	B_r (Tesla)	B_r (Theory)
.100	.9725E-03	.1941E-02	.1047E-04	.3640E-04
.300	.9757E-03	.1940E-02	.3192E-04	.1097E-03
.500	.9824E-03	.1939E-02	.5361E-04	.1843E-03
.700	.9933E-03	.1937E-02	.7572E-04	.2614E-03
.900	.1010E-02	.1933E-02	.9837E-04	.3420E-03
1.100	.1034E-02	.1928E-02	.1215E-03	.4276E-03
1.300	.1069E-02	.1920E-02	.1444E-03	.5198E-03
1.500	.1124E-02	.1909E-02	.1637E-03	.6208E-03
1.700	.1212E-02	.1891E-02	.1641E-03	.7337E-03
1.900	.1332E-02	.1862E-02	.8745E-04	.8623E-03

BFLUX = .915E-05 WEBERS
Corrected BFLUX = .913E-05 WEBERS
Theoretical BFLUX = .155E-04 WEBERS

Z = .95 INCHES

Radius (cm)	B_z (Tesla)	B_z (Theory)	B_r (Tesla)	B_r (Theory)
.050	.3659E-02	.2981E-02	.5050E-04	-.9566E-05
.150	.3671E-02	.2982E-02	.1507E-03	-.2871E-04
.250	.3696E-02	.2986E-02	.2546E-03	-.4788E-04
.350	.3738E-02	.2991E-02	.3651E-03	-.6711E-04
.450	.3802E-02	.2998E-02	.4859E-03	-.8641E-04
.550	.3897E-02	.3007E-02	.6223E-03	-.1058E-03
.650	.4044E-02	.3018E-02	.7819E-03	-.1253E-03
.750	.4290E-02	.3031E-02	.9757E-03	-.1449E-03
.850	.4769E-02	.3045E-02	.1205E-02	-.1646E-03
.950	.6023E-02	.3062E-02	.1149E-02	-.1844E-03

BFLUX = .910E-05 WEBERS
Corrected BFLUX = .897E-05 WEBERS
Theoretical BFLUX = .613E-05 WEBERS

Z = 0.00 INCHES

Radius (cm)	B_z (Tesla)	B_z (Theory)	B_r (Tesla)	B_r (Theory)
.050	.4427E-02	.2473E-02	.1927E-06	-.1654E-04
.150	.4433E-02	.2474E-02	.3840E-07	-.4968E-04
.250	.4443E-02	.2476E-02	-.1156E-06	-.8297E-04
.350	.4457E-02	.2479E-02	-.2690E-06	-.1165E-03
.450	.4474E-02	.2484E-02	-.4335E-06	-.1504E-03
.550	.4492E-02	.2489E-02	-.5951E-06	-.1848E-03
.650	.4509E-02	.2495E-02	-.7499E-06	-.2197E-03
.750	.4524E-02	.2503E-02	-.9096E-06	-.2554E-03
.850	.4535E-02	.2511E-02	-.1065E-05	-.2919E-03
.950	.4541E-02	.2522E-02	.1065E-05	-.3293E-03

BFLUX = .913E-05 WEBERS
Corrected BFLUX = .905E-05 WEBERS
Theoretical BFLUX = .507E-05 WEBERS

Z = -0.95 INCHES

Radius (cm)	B_z (Tesla)	B_z (Theory)	B_r (Tesla)	B_r (Theory)
.050	.3657E-02	.1797E-02	-.5011E-04	-.1790E-04
.150	.3669E-02	.1796E-02	-.1505E-03	-.5375E-04
.250	.3695E-02	.1795E-02	-.2545E-03	-.8975E-04
.350	.3737E-02	.1794E-02	-.3651E-03	-.1260E-03
.450	.3800E-02	.1792E-02	-.4859E-03	-.1626E-03
.550	.3896E-02	.1790E-02	-.6223E-03	-.1997E-03
.650	.4043E-02	.1787E-02	-.7819E-03	-.2373E-03
.750	.4289E-02	.1783E-02	-.9756E-03	-.2756E-03
.850	.4767E-02	.1779E-02	-.1204E-02	-.3148E-03
.950	.6001E-02	.1774E-02	-.1146E-02	-.3549E-03

BFLUX = .909E-05 WEBERS
Corrected BFLUX = .896F-05 WEBERS
Theoretical BFLUX = .362E-05 WEBERS

Z = -4.75 INCHES

Radius (cm)	B_z (Tesla)	B_z (Theory)	B_r (Tesla)	B_r (Theory)
.100	.9245E-03	.3292E-03	-.1316E-04	-.6615E-05
.300	.9284E-03	.3278E-03	-.3951E-04	-.1979E-04
.500	.9365E-03	.3252E-03	-.6630E-04	-.3279E-04
.700	.9498E-03	.3213E-03	-.9382E-04	-.4551E-04
.900	.9700E-03	.3161E-03	-.1223E-03	-.5785E-04
1.100	.1000E-02	.3097E-03	-.1518E-03	-.6968E-04
1.300	.1045E-02	.3022E-03	-.1812E-03	-.8093E-04
1.500	.1115E-02	.2937E-03	-.2061E-03	-.9148E-04
1.700	.1227E-02	.2841E-03	-.2068E-03	-.1013E-03
1.900	.1379E-02	.2738E-03	-.1101E-03	-.1102E-03

BFLUX = .909E-05 WEBERS
Corrected BFLUX = .907E-05 WEBERS
Theoretical BFLUX = .242E-05 WEBERS
